This is the accepted author's version of the manuscript. Final edited version can be found at https://ieeexplore.ieee.org/document/8719630
doi: 10.1109/WEARRACON.2019.8719630

Preliminary Investigation of Symmetry Learning Control for Powered Ankle-Foot Prostheses

Jonathan Realmuto, Glenn Klute, and Santosh Devasia

***Abstract*— This article proposes a human-in-the-loop optimization method, targeting gait symmetry, for powered ankle-foot prostheses (PAFPs). Individuals with unilateral below-knee amputations have distinctly asymmetrical gaits, which predisposes them to a host of secondary musculoskeletal impairments, including osteoarthritis of the intact limb joints. PAFPs can restore some ankle function, however current control methodologies rely on able-bodied gait data for trajectory synthesis, require expert tuning, and are limited in their ability to adapt. Human-in-the-loop methods, where the control signal is adjusted based on the achieved actions of the coupled human-robot system, would allow for automatic personalization and continuous adaptation. An adaptive gain iterative learning control algorithm adjusts the PAFPs torque to match the achieved intact ankle torque while maintaining boundedness of the control signal. The method is experimentally assessed during a pilot (N=1) study with a prototype PAFP. Results indicate a 25% reduction in the difference of mean peak ankle torques, and a reduction in ankle toque, ankle power and support moment asymmetry. This work demonstrates the practical implementation of a symmetry-based learning controller, which resulted in beneficial biomechanic adaptations, therefore providing motivation for future investigations of symmetry-based controllers for PAFPs.**

I. Introduction

One of the most significant consequences of below-knee amputations is asymmetrical loading of the lower limbs during ambulation, which predisposes individuals to secondary conditions [1], including osteoarthritis (OA) in their intact knee and hip joints, and osteopenia and osteoporosis in the residual limb [2]. The inability to actively produce ankle power results in a variety of neuromuscular adaptations [3], including spending less time in stance phase on their prosthetic limb [4], loading their prosthetic limb less that their intact limb [5], loading their intact limb more relative to people without lower-limb amputations [6], and increased hip extension and knee flexion in the intact limb [7]. Prostheses with improved push-off characteristics can reduce biomechanical risk factors linked to OA [8], therefore power ankle-foot prostheses (PAFPs) may prevent secondary musculoskeletal conditions.

*This work was supported by the U.S. Department of Veterans Affairs, Rehabilitation Research and Development Service, Grants A9248-S and A9243C, and by the U.S. Department of Education (GAANN P200A130025)

J. Realmuto is with the Department of Biomedical Engineering, Viterbi School of Engineering, University of Southern California. realmuto@usc.edu

G. Klute is with the Department of Veterans Affairs, Center for Limb Loss and Mobility, and the Department of Mechanical Engineering, University of Washington. gklute@uw.edu

S. Devasia is with the Department of Mechanical Engineering, University of Washington. sdevasia@uw.edu

PAFPs can potentially replicate human ankle behavior, however, adequately mimicking the natural functions of the human ankle is challenging and control of PAFPs is an active area of research, see e.g., [9]. A common approach is to use state-based controllers, where each state alters the ankle mechanics (i.e., impedance) of the prosthesis with parameters derived from able-bodied human ankle mechanics [10]–[12]. Another approach is to encode the motor command signal, derived from able-bodied data, as a time-based function that initiates on heel-strike (HS) [13]. A reflex controller, based on a neuromuscular model fitted to match the human ankle torque-angle profile of weight and height-matched intact subjects, can provide some adaptation to slope changes [14]. These approaches are limited by: (i) able-bodied trajectories do not account for personalized altered body mechanics of amputee gait, (ii) the need for (expert) qualitative tuning of subject specific control parameters, and (iii) an inability to automatically adapt to the user. Gait mechanics and muscle activity vary widely across individuals [15], thus able-bodied push-off work should not be the only consideration when formulating control trajectories. Methods for the automatic tuning of lower-limb powered prostheses impedance parameters are beginning to emerge [16]. However, the optimization features which benefit the user most is still unclear [15].

Human-in-the-loop methods, where the control signal is automatically tuned, could overcome the limitations outlined above. Such methods have proved successful at minimizing walking economy with ankle exoskeletons [17], [18]. Additionally, these methods have provided insights into the need for personalization, evident from the large variations in optimized assistance found across individuals [18]. However, in the case of human-in-the-loop methods for PAFPs, identifying a measurable user-related metric, e.g., comfort or satisfaction, is not straightforward. The relationship between activity limitations and the metabolic cost in the amputee population remains unclear [19], thus walking economy may not be an ideal candidate for optimization. Additionally, research suggests that PAFPs may not significantly effect metabolic cost [15], [20]. Alternatively, in this work, ankle torque symmetry is proposed as a candidate for optimization. The challenge, as with any in human-in-the-loop approach, is to avoid divergent responses cause by time-varying human dynamics.

The main contribution of this work is a personalized symmetry learning controller that reduces ankle torque asymmetry. The method utilizes the adaptive gain iterative learning control (AG-ILC) algorithm [21], and can avoid divergent responses caused by unmodeled human dynamics. The al-

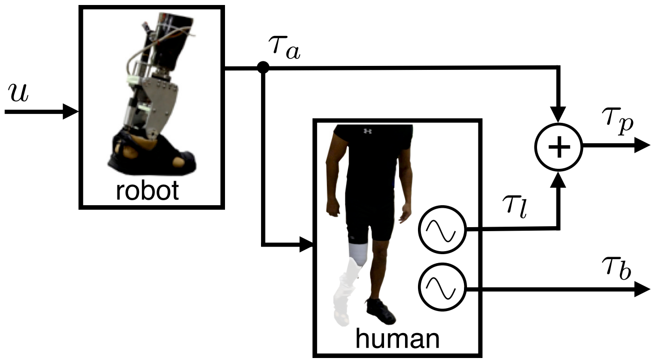

Fig. 1: Conceptual model illustrating the research problem. The goal is to find the control signal u such that the active torque τ_a, summed with the (loading) passive torque τ_l, results in a total prosthetic torque τ_p that matches the biological (intact) torque τ_b.

gorithm learns a command signal by iteratively reducing torque asymmetries of the prosthetic and intact limbs in the frequency domain. Divergence is avoided by monitoring the difference between the prosthetic and intact ankle torques and adjusting the frequency dependent learning gain accordingly. The proposed method is experimentally assessed with a prototype PAFP. To eliminate the need for real-time torque estimates, standard inverse dynamics provide ankle torques to the AG-ILC algorithm, which is updated off-line between walking trials. We hypothesize that the symmetry control method will result in (1) a decrease in ankle kinematic and kinetic asymmetries, and (2) a decrease in support moment asymmetry, which has been shown to have a more consistent pattern than any one individual joint [22].

II. Symmetry Control

A. Problem Formulation

1) Model Abstraction: The conceptual model in Fig. 1 illustrates the research problem: choose the control signal u such that the prosthetic torque τ_p matches the biological (intact) ankle torque τ_b, i.e.,

$$\tau_p(t) = \tau_b(t), \tag{1}$$

where t in (1) represents the time-normalized gait cycle. The PAFP (robot) takes as an input the control signal u and outputs an active torque τ_a about the prosthetic ankle joint. In addition, the prosthesis provides a loading torque τ_l (i.e., from the passive dynamics), which sum with the active torque τ_a to produce the total prosthetic torque τ_p,

$$\tau_p(t) = \tau_l(t) + \tau_a(t). \tag{2}$$

The active torque τ_a effects both the loading torque τ_l and the biological torque τ_b through the human-response dynamics, which can vary depending on the individual.

2) Iterative Learning Control: The iterative learning control (ILC) approach is to update the motor current command u at each iteration k (in the frequency domain):

$$u_{k+1}(\omega) = u_k(\omega) + \rho_k(\omega) G_m^{-1}(\omega) e_k(\omega), \tag{3}$$

where ρ_k is the learning gain, e_k is the error signal, and G_m is a model of the robot dynamics

$$G_m(\omega) = \frac{\tau_a(\omega)}{u(\omega)}. \tag{4}$$

The error signal e_k in (3) is taken as the difference between the time-normalized mean biological torque and the mean prosthetic torque,

$$e_k(\omega) = \bar{\tau}_{b,k}(\omega) - \bar{\tau}_{p,k}(\omega), \tag{5}$$

and represents a measure of ankle torque asymmetry. Mean torque signals at each iteration k are computed over a walking trial, taking the mean value at each discrete percent gait cycle over all steps.

3) ILC Convergence: Ideally, repetitive application of the update law in (3) will result in convergence of the error signal in (5), e.g.,

$$\lim_{k \to \infty} |e_k(\omega)| = 0. \tag{6}$$

Convergence of (3) can be achieved at each frequency ω provided: (i) the phase error in the model G_m and the choice of learning gain ρ_k are sufficiently small, and (ii) the reference signal (i.e., $\bar{\tau}_{b,k}$ in this case) is fixed [23]. Since the control signal u affects the biological torque τ_b the reference signal can vary according to the personalized human-response dynamics, and thus it may not be possible to guarantee convergence.

4) Avoiding Divergence: The problem investigated is the selection of the frequency-dependent learning gain ρ_k such that the control signal u remains bounded. Boundedness of the control signal u is critical for safety. Simply applying the update law in (3) with a fixed learning gain $\rho_k(\omega) = \rho(\omega)$ could result in an unbounded control signal u_k. Another scenario is that the magnitude of the error signal in (5) could decrease at each iteration k, but the magnitudes of each torque component, prosthetic torque $\bar{\tau}_{p,k}$ and biological torque $\bar{\tau}_{b,k}$, could increase at each iteration k. Such a scenario would lead to unbounded growth of the control signal u, and poses a safety issue for the user.

B. Adaptive Gain ILC

To address the problems outline above, this work proposes an adaptive gain technique, which monitors the error and the reference signals growth and adapts the frequency dependent learning gain ρ_k. There are three components to the AG-ILC algorithm: (i) conditional statements that determine how the algorithm updates, (ii) a cache that stores the algorithm's internal states, and (iii) the update law that results in a new control signal u_{k+1}. Each component is described below.

1) Update Conditions: Three update conditions, stored as boolean variables, determine how the update law evolves. The first condition $\mathcal{C}_{1,k}$ determines if the error signal e_k is smaller in magnitude than the previously smallest observed error signal e^*_{k-1},

$$\mathcal{C}_{1,k}(\omega) = \begin{cases} 1 & \text{if} \quad |e_k(\omega)| < |e^*_{k-1}(\omega)| \\ 0 & \text{else} \end{cases}. \tag{7}$$

Another condition, $\mathcal{C}_{2,k}$, determines if the error signal is larger in magnitude than the previously smallest observed error signal e^*_{k-1} plus padding ϵ,

$$\mathcal{C}_{2,k}(\omega) = \begin{cases} 1 & \text{if} \quad |e_k(\omega)| > |e^*_{k-1}(\omega)| + \epsilon(\omega) \\ 0 & \text{else} \end{cases} \tag{8}$$

where the frequency dependent padding $\epsilon(\omega)$ is an estimate of the expected variation in the error signal e_k, (i.e., a noise estimate). The final condition $\mathcal{C}_{3,k}$ determines if the reference signal $\bar{\tau}_{b,k}$ has grown larger in magnitude than a scaled version of the initial error e_0. The change in reference signal is computed as

$$\Delta\tau_{b,k}(\cdot) = \bar{\tau}_{b,k}(\cdot) - \bar{\tau}_{b,0}(\cdot), \tag{9}$$

and the final condition is

$$\mathcal{C}_{3,k}(\omega) = \begin{cases} 1 & \text{if} \quad |\Delta\tau_{b,k}(\omega)| > \alpha|e_0(\omega)| \\ 0 & \text{else} \end{cases} \tag{10}$$

where the constant α represents the allowable growth of the change in reference signal $\Delta\tau_{b,k}$ relative to the initial error e_0.

2) Cache: The cache updates and stores the state of the algorithm, based on the conditions outlined above, as follows:

$$\rho_k(\omega) = \begin{cases} \frac{1}{\gamma}\rho_{k-1}(\omega) & \text{if } \mathcal{C}_{2,k}(\omega) + \mathcal{C}_{3,k}(\omega) > 0 \\ \rho_{k-1}(\omega) & \text{else} \end{cases} \tag{11}$$

$$e^*_k(\omega) = \begin{cases} e_k(\omega) & \text{if } \mathcal{C}_{1,k}(\omega) = 1 \text{ and } \mathcal{C}_{3,k}(\omega) = 0 \\ e^*_{k-1}(\omega) & \text{else} \end{cases} \tag{12}$$

$$u^*_k(\omega) = \begin{cases} u_k(\omega) & \text{if } \mathcal{C}_{1,k}(\omega) = 1 \text{ and } \mathcal{C}_{3,k}(\omega) = 0 \\ u^*_{k-1}(\omega) & \text{else} \end{cases} \tag{13}$$

where $\gamma > 1$ determines the decay rate of the learning gain ρ_k if a sufficient increase in the error signal e_k is observed (condition $\mathcal{C}_{2,k}$ defined in (8)) or a sufficient increase in the reference signal $\tau_{b,k}$ is observed (condition $\mathcal{C}_{3,k}$ defined (10)). The frequency dependent padding ϵ in (8) allows the error signal to fluctuate within the expected noise region without penalty to the learning gain ρ_k. Additionally, e^*_k in (12) and u^*_k in (13) are updated if and only if the magnitude of the error e_k is strictly decreasing (condition $\mathcal{C}_{1,k}$ defined (7)) and the magnitude of the reference signal $\bar{\tau}_{b,k}$ remains bounded by the initial error e_0 (condition $\mathcal{C}_{3,k}$ defined (10)).

3) AG-ILC Update Law: The update law utilizes the cached values, outlined in (11)-(13), to determine the new control signal $\hat{u}_{k+1}$, as:

$$\hat{u}_{k+1}(\omega) = u^*_k(\omega) + \rho_k(\omega) G_m^{-1}(\omega) e^*_k(\omega). \tag{14}$$

During initial contact and swing phase the control signal in (14) is set to zero,

$$\tilde{u}_{k+1}(t) = \begin{cases} 0 & \text{if } (t < t_1) \text{ or } (t > t_2) \\ \hat{u}_{k+1}(t) & \text{otherwise} \end{cases}, \tag{15}$$

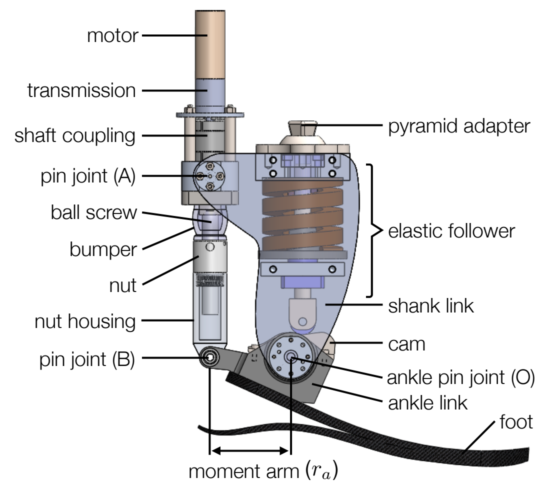

Fig. 2: Illustrative rendering of the prototype PAFP with major components labeled (note some components are transparent for ease in visualization).

where t_1 and t_2 define the time region for non-zero control signal. Finally, the new control signal u_{k+1} is found as

$$u_{k+1}(\omega) = \zeta(\tilde{u}_{k+1}(\omega)) \tag{16}$$

where ζ represents a zero-phase low-pass filter with cutoff frequency ω_c that smooths the signal.

III. Prototype Ankle-Foot Prosthesis

The prototype PAFP, shown in Fig. 2, is a nonlinear parallel elastic actuator. A cam-based spring [24] acts across the ankle joint, providing nonlinear elasticity parallel with the powered drive train. An energy store and return passive foot (Ossur LP Vari-Flex), attached to the ankle link, protects the drive train from shocks and provides additional energy storing and releasing capability.

A. Drive Train Model

The powered drive train, a motorized link acting across the shank and ankle links (see Fig. 2), provides the active torque τ_a, defined in (2). The drive train consists of the following: a brushless DC motor (Maxon EC-22, 100 W, 24 V), attached to a pin joint on the shank link (pin joint (A)), in series with a planetary gearhead with a transmission ratio of $R_g = 19$ (Maxon GP 22 HP), followed by $\ell = 4$ mm pitch linear ball screw (Thompson NEFF Rolled Ball Screw) attached to a pin joint on the ankle link (pin joint (B)) that acts with a moment arm $r_a = 6$ mm from the ankle joint (ankle pin joint (O)). A compliant bumper (polyester/rubber blend with a durometer hardness rating of 40D), located between the ball screw nut and ball screw housing, protects the transmission from shocks, i.e., it engages near maximum plantarflexion. The robot model G_m in (14) is taken as the effective transmission gain from the motor current i_a to the active torque τ_a, found by combining each stage of the transmission:

$$G_m = \eta_s \eta_g r_a R_g \frac{2\pi}{\ell} k_\tau, \tag{17}$$

where k_τ is the torque constant of the motor, η_s is the ball screw efficiency, and η_g the gearhead efficiency.

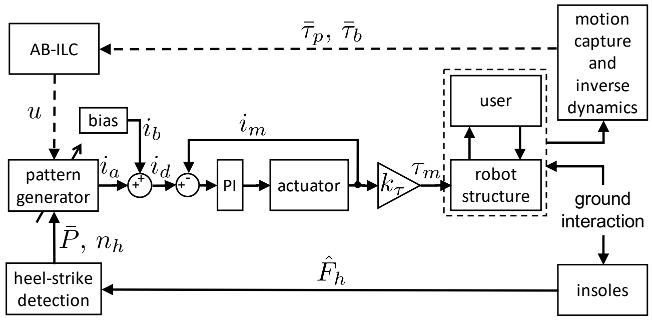

Fig. 3: Block diagram of controller architecture. Solid lines represent real-time signals and dashed lines represent off-line signals.

B. Controller Architecture

The controller architecture is illustrated as a block diagram in Fig. 3. The embedded system, which operates in real-time, utilizes an insole force sensor signal $\hat{F}_h$ to identify the time-stamp n_h of the most recent HS, and estimates the mean step period $\bar{P}$. Next, a pattern generator (i.e., lookup table) is used to modulating the active motor current i_a based on the most recent heel-strike time-stamp n_h and mean step period $\bar{P}$. The bias current i_b in Fig. 3 adjusts the equilibrium position of the PAFP and can be chosen by the user. Additionally, a low-level proportional-integral (PI) controller is used to track the desired motor current i_d. Offline, after each walking trial (e.g., learning iteration k), inverse dynamics are computed on the motion capture (MoCap) data, resulting in the mean prosthetic torque $\bar{\tau}_{p,k}$ and mean biological torque $\bar{\tau}_{b,k}$. Finally, the mean torque signals are used to compute the error signal e_k defined in (5), and subsequently, using the AG-ILC algorithm outlined in Sect. II-B, a new control signal u_{k+1} defined in (16), is then encoded in the pattern generator.

IV. Experimental Methods

The purpose of the pilot (N=1) study was to provide a preliminary investigation of whether the proposed method is a viable control paradigm for PAFPs, with the goal of quantifying the effect of symmetry control compared with passive mode. The experimental setup consisted of a split-belt force-sensing treadmill (Bertec), a 12-camera MoCap system (Vicon), and a human subject donning the PAFP with custom embedded system and tethered power supply. A plug-in gait model, consisting of 36 reflective markers, was used to compute inverse dynamics. The prototype PAFP was fitted to left leg of the subject, using their as-prescribed socket and suspension system, and aligned by a certified prosthetist. The subject provided written informed consent to participate in the experimental protocol, approved by the VA Institutional Review Board. The subject was a healthy, active 85 kg unilateral below-knee amputee. Table I provides details of the subject's characteristics.

A. Protocol

Before ambulating, the subject was asked to choose a neutral position of the PAFP that was most comfortable during standing. The process, similar to alignment procedures used for conventional prosthetic feet and supervised by the prosthetist, was accomplished by modulating the bias current i_b, shown in Fig. 3. Next, the subject acclimated to the PAFP by walking on the treadmill for approximately 5 minutes at their self-selected treadmill walking speed (1 m/s). After acclimation, the experimental trials commenced, where each learning iteration k consisted of 30 seconds of steady state walking. After each learning iteration k, the subject was allowed to sit down while data was processed, the AG-ILC algorithm was executed and a new control law uploaded to the embedded system (approximately $4{-}5$ minutes). Prior to collecting the next trial, the subject first began ambulating in passive mode. Next, the control signal was introduced to the user over the course of $40{-}80$ strides (i.e., by linearly scaling the signal). After the subject acclimated to the new control signal ($\sim$30 seconds), data was collected. This process was repeated until the measured error signal e_k could no longer be reduced.

B. Quantifying Asymmetry

Asymmetry was quantified as the root-mean-square difference between the mean time-normalized waveforms, (e.g., mean at each percent gait over all steps) of each limb variable.

$$\text{AM} = \sqrt{\frac{1}{p}\sum_{1}^{p}(x_i - y_i)^2} \tag{18}$$

where p is the number of points used for time-normalization, x represents the mean right limb gait variable (i.e., right ankle torque) and y represents mean the left limb gait variable (i.e., left ankle torque). Asymmetry increases with increasing value of (18), with a value of zero corresponding to perfectly symmetrical.

V. Results and Discussion

The experiment consisted of 10 walking trials (iterations): one passive trial ($k = 0$) and nine trials ($k = 1{-}9$) where the PAFP was active. In the following, the $k = 0$ passive trial ("Passive" condition) is compared to the final $k = 9$ trial ("Symmerty" condition).

A. Algorithm Performance

Despite human adaptations, the AG-ILC algorithm resulted in bounded control signals u_k for all iterations k. This can be seen in Fig. 4, which shows time-domain signal traces at each iteration k for the active torque, estimated as

$$\hat{\tau}_{a,k}(t) = R_T \cdot k_\tau \cdot u_k(t), \tag{19}$$

TABLE I: Subject characteristics.

Gender	male
Age (yrs)	50
Height (cm)	180
Intact leg length (mm)	900
Mass prescribed (kg)	82
Mass prototype (kg)	85
Etiology	traumatic
Prescribed prosthesis	Ossur Pro-Flex XC

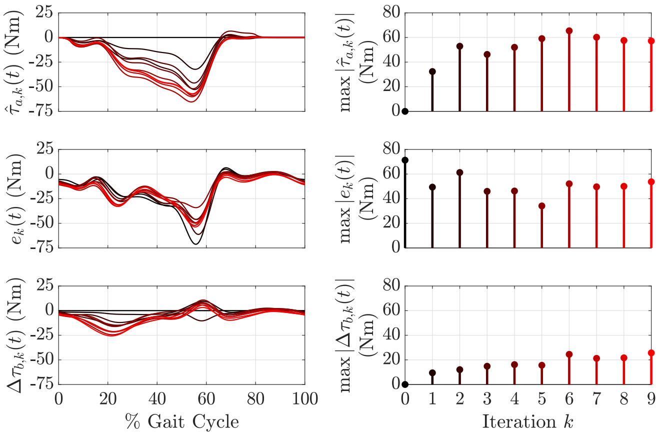

Fig. 4: Algorithm performance during each iteration k. Time domain signals (left column): (top) estimated active torque $\hat{\tau}_{a,k}$ defined in (19); (middle) error e_k defined in (5); (bottom) change in reference signal $\Delta\tau_{b,k}$ defined in (9). Peak values for each iteration (right column): (top) peak estimated active torque $\hat{\tau}_{a,k}$; (middle) peak error e_k; (bottom) peak change in reference signal $\Delta\tau_{b,k}$. Note the color of the traces corresponds to each iteration k (gradient from black ($k = 0$) to red ($k = 9$)).

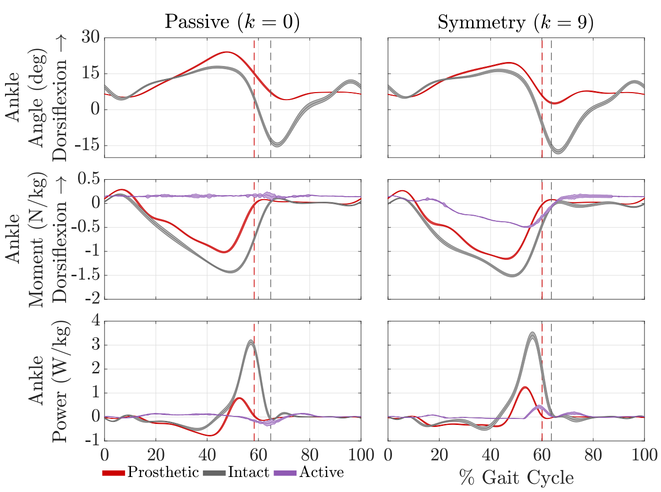

Fig. 5: Ankle angle (top row), moment (middle row) and power (bottom row) for passive condition (left column) and symmetry condition (right column). Dashed vertical lines in ankle mechanics plots denote TO. Traces labeled "Active" represent the active torque $\hat{\tau}_{a,k}$, defined in (19), and active power, defined in (20). Thickness of each traces represents $\pm$ 1 standard deviation.

(top-left plot), the error e_k (defined in (5)) (middle-left plot), and the change in reference signal $\Delta\tau_{b,k}$ (defined in (9)) (bottom-left plot). Additionally, the corresponding right column plots show each signals respective peak value, e.g, $\max|\cdot|$, for each iteration k. The evolution of the active torque $\hat{\tau}_{a,k}$ was consistent with the error e_k: if the error e_k increased in magnitude relative to the previous iteration, the active torque decreased on the following iteration, as expected. The lowest achieved peak error e_k, a reduction of 52%, occur at iteration $k = 5$. However, the peak error e_k increased in subsequent iterations, and a reduction of 25% was observed during the final iteration ($k = 9$).

B. Ankle Asymmetry

1) Angle: The proposed method increased ankle angle asymmetry, calculated using (18), from 7.63° during the passive condition ($k = 0$) to 7.71° during the symmetry ($k =$ 9) condition, corresponding to a 1% increase in asymmetry (Table II). The mean ankle angle (and $\pm$1 standard deviation) for each condition top row of Fig. 5.

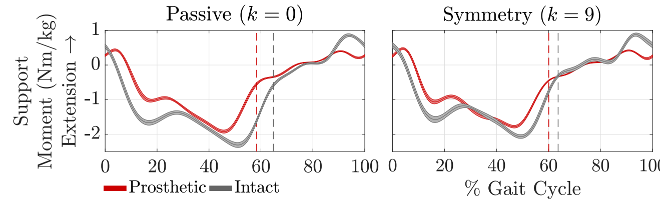

Fig. 6: Support moment for passive condition (left column) and symmetry condition (right column). Vertical lines in plots denote TO. Thickness of each traces represents $\pm$ 1 standard deviation.

2) Moment: The proposed method decreased the ankle moment asymmetry, computed as in (18), from a 0.30 (Nm/kg) during the passive condition to a mean of 0.26 (Nm/kg) during the symmetry condition, corresponding to a 14% reduction in ankle moment asymmetry (see Table II). The middle row of Fig. 5 shows the mean ankle moment for each condition, including the active torque $\hat{\tau}_{a,k}$ (defined in (19)) contribution. The active torque supplied during the symmetry condition altered the mean stance period of gait on both the prosthetic and intact sides: the prosthetic side mean stance period increase from 58% to 60% of the gait cycle, while the intact side decreased from 65% to 64% of the gait cycle. This can be seen in Fig. 5 as the dash vertical lines corresponding to TO.

3) Power: Ankle power asymmetry, computed as in (18), decreased during the symmetry condition from 0.71 W/kg to 0.67 W/kg, corresponding to a 6% reduction in asymmetry. The ankle power asymmetry outcomes are recorded in Table II. The bottom row of Fig. 5 shows the mean ankle power for each condition, including the active power contribution. The active power was calculated as:

$$P_a = k_\tau \cdot i_m \cdot \omega_m \tag{20}$$

where k_τ was the torque constant, i_m the motor current, and ω_m the motor angular velocity. The most apparent modification was an increase in intact peak power, from 3.12 W/kg during the passive condition to 3.41 W/kg during the symmetry condition (9% increase).

C. Support Moment Asymmetry

Support moment asymmetry ($\tau_{SM} = \tau_{ankle} + \tau_{knee} + \tau_{hip}$) reduced during the symmetry condition, from 0.52 (Nm/kg) to 0.35 (Nm/kg), a 32% decrease (see Table II). Figure 6 shows mean support moment for each condition. The symmetry control largely influenced the knee and hip mechanics on both the prosthetic and intact sides, decreases

TABLE II: Asymmetry outcome measures,defined in (18).

	Passive ($k = 0$)	Symmetry ($k = 9$)	% Change
Angle (deg)	7.63	7.71	1.09%
Moment (Nm/kg)	0.30	0.26	13.86%
Power (W/kg)	0.71	0.67	5.80%
Support Moment (Nm/kg)	0.52	0.35	31.89%

the peak support moment on the intact side, which can be seen in Fig. 6 at around 50% of the gait cycle. It's well known that many compensatory behaviors occur at the knee and hip of the intact side [7]. This result suggests that a modest decrease in ankle torque asymmetry can produce considerable beneficial adaptations in the other joints.

D. Limitations and Future Directions

A limitation of the proposed approach is the use of (off-line) inverse dynamics for estimating ankle torque symmetry. Consequently, users are restricted to training in a laboratory setting, where the learning algorithm can be executed. Estimating lower-limb biomechanics in real-time, using model-based approaches or machine learning techniques, is critical for future embodiments. Additionally, the use of a rigid body MoCap model to calculate ankle-foot position, torque, and power is limiting, and our future work will include more precise models [25]. The current experimental protocol is the relatively short acclimation period and rapid changes in the ambulatory condition, which may not be conducive to acquiring a novel gait pattern. In prior studies, participants acclimate during a period of several weeks [8]. A long term learning approach, where the learning iterations occur over the course of a day (or more), would allow more time for the user to converge to each new condition (learning iteration). Improvements are possible to the current prototype PAFP, as it is heavy ($\sim$3 kg), tethered to a power supply and has limited memory storage for encoding control signals.

VI. Conclusion

This work proposed a human-in-the-loop controller, for powered ankle-foot prostheses, targeting gait asymmetry. The method corrected the active ankle torque of the prosthetic limb to match the achieved ankle toque of the intact limb by utilizing an adaptive gain iterative learning control algorithm. We hypothesized that the method would result in (1) a reduction in sagittal plane ankle kinetic and kinematic asymmetry, and (2) a reduction in the support moment asymmetry. A preliminary experimental pilot study was conducted. The results show a 25% reduction in peak torque difference (Fig. 4), a significant reduction in ankle moment (14%) and power asymmetries (6%), and an increase in ankle angle asymmetry (1%) (Fig. 5), and a significant reduction in support moment asymmetry (32%) (Fig. 6). These results provide a proof-of-concept demonstration that targeting symmetry for human-in-the-loop optimization of powered ankle-foot prostheses can improve gait symmetry, and motivates future investigation of symmetry-based controllers.

References

[1] D. C. Morgenroth, A. C. Gellhorn, and P. Suri, "Osteoarthritis in the disabled population: a mechanical perspective," *PM&R*, vol. 4, no. 5, pp. S20–S27, 2012.

[2] R. Gailey, K. Allen, J. Castles, J. Kucharik, and M. Roeder, "Review of secondary physical conditions associated with lower-limb amputation and long-term prosthesis use," *J. Rehabil. Res. Dev.*, vol. 45, no. 1, p. 15, 2008.

[3] P. Adamczyk and A. Kuo, "Mechanisms of gait asymmetry due to push-off deficiency in unilateral amputees," *IEEE Trans. Neural Syst. Rehabil. Eng.*, vol. 23, no. 5, pp. 776–785, Sept 2015.

[4] D. J. Sanderson and P. E. Martin, "Lower extremity kinematic and kinetic adaptations in unilateral below-knee amputees during walking," *Gait & Posture*, vol. 6, no. 2, pp. 126–136, 1997.

[5] R. D. Snyder, C. M. Powers, C. Fontaine, and J. Perry, "The effect of five prosthetic feet on the gait and loading of the sound limb in dysvascular below-knee amputees," *J. Rehabil. Res. Dev.*, vol. 32, no. 4, p. 309, 1995.

[6] J. Engsberg, A. Lee, K. Tedford, and J. Harder, "Normative ground reaction force data for able-bodied and below-knee-amputee children during walking." *J. Pediatr. Orthop.*, vol. 13, no. 2, pp. 169–173, 1992.

[7] H. Bateni and S. J. Olney, "Kinematic and kinetic variations of below-knee amputee gait," *J. Prosthet. Orthot.*, vol. 14, no. 1, pp. 2–10, 2002.

[8] E. R. Esposito and J. M. Wilken, "Biomechanical risk factors for knee osteoarthritis when using passive and powered ankle–foot prostheses," *Clin. Biomech.*, vol. 29, no. 10, pp. 1186–1192, 2014.

[9] R. Jimenez-Fabian and O. Verlinden, "Review of control algorithms for robotic ankle systems in lower-limb orthoses, prostheses, and exoskeletons," *Med. Eng. Phys.*, vol. 34, no. 4, pp. 397–408, 2012.

[10] S. K. Au, J. Weber, and H. Herr, "Powered ankle–foot prosthesis improves walking metabolic economy," *IEEE Trans. Robot.*, vol. 25, no. 1, pp. 51–66, 2009.

[11] A. H. Shultz, B. E. Lawson, and M. Goldfarb, "Variable cadence walking and ground adaptive standing with a powered ankle prosthesis," *IEEE Trans. Neural Syst. Rehabil. Eng.*, vol. 24, no. 4, pp. 495–505, 2016.

[12] P. Cherelle, V. Grosu, L. Flynn, K. Junius, M. Moltedo, B. Vanderborght, and D. Lefeber, "The ankle mimicking prosthetic foot 3locking mechanisms, actuator design, control and experiments with an amputee," *Rob. Auton. Syst.*, vol. 91, pp. 327–336, 2017.

[13] J. K. Hitt, T. G. Sugar, M. Holgate, and R. Bellman, "An active foot-ankle prosthesis with biomechanical energy regeneration," *J. Med. Device.*, vol. 4, no. 1, p. 011003, 2010.

[14] M. F. Eilenberg, H. Geyer, and H. Herr, "Control of a powered ankle–foot prosthesis based on a neuromuscular model," *IEEE Trans. Neural Syst. Rehabil. Eng.*, vol. 18, no. 2, pp. 164–173, 2010.

[15] R. E. Quesada, J. M. Caputo, and S. H. Collins, "Increasing ankle push-off work with a powered prosthesis does not necessarily reduce metabolic rate for transtibial amputees," *J. Biomech.*, vol. 49, no. 14, pp. 3452–3459, 2016.

[16] H. Huang, D. L. Crouch, M. Liu, G. S. Sawicki, and D. Wang, "A cyber expert system for auto-tuning powered prosthesis impedance control parameters," *Ann. Biomed. Eng.*, vol. 44, no. 5, pp. 1613–1624, 2016.

[17] J. R. Koller, D. H. Gates, D. P. Ferris, and C. D. Remy, "'body-in-the-loop' optimization of assistive robotic devices: A validation study." in *Robotics: Science and Systems*, 2016.

[18] J. Zhang, P. Fiers, K. A. Witte, R. W. Jackson, K. L. Poggensee, C. G. Atkeson, and S. H. Collins, "Human-in-the-loop optimization of exoskeleton assistance during walking," *Science*, vol. 356, no. 6344, pp. 1280–1284, 2017.

[19] J. M. Czerniecki and D. C. Morgenroth, "Metabolic energy expenditure of ambulation in lower extremity amputees: what have we learned and what are the next steps?" *Disabil. Rehabil.*, vol. 39, no. 2, pp. 143–151, 2017.

[20] E. S. Gardinier, B. M. Kelly, J. Wensman, and D. H. Gates, "A controlled clinical trial of a clinically-tuned powered ankle prosthesis in people with transtibial amputation," *Clin. Rehabil.*, vol. 32, no. 3, pp. 319–329, 2018.

[21] J. Realmuto, R. B. Warrier, and S. Devasia, "Iterative learning control for human-robot collaborative output tracking," in *Proc. IEEE/ASME 12th Int. Conf. Mechatronic and Embedded Systems and Applications (MESA)*. IEEE, 2016, pp. 1–6.

[22] D. A. Winter, "Overall principle of lower limb support during stance phase of gait," *J. Biomech.*, vol. 13, no. 11, pp. 923–927, 1980.

[23] S. Tien, Q. Zou, and S. Devasia, "Iterative control of dynamics-coupling-caused errors in piezoscanners during high-speed afm operation," *IEEE Trans. Control. Syst. Technol.*, vol. 13, no. 6, pp. 921–931, 2005.

[24] J. Realmuto, G. Klute, and S. Devasia, "Nonlinear passive cam-based springs for powered ankle prostheses," *J. Med. Device.*, vol. 9, no. 1, p. 011007, 2015.

[25] K. E. Zelik and E. C. Honert, "Ankle and foot power in gait analysis: Implications for science, technology and clinical assessment," *J. Biomech.*, 2018.